Lasers in Manufacturing Conference 2019

Microstructure and Mechanical Characterization of Laser Aided Additive Manufactured Fe50Mn30Co10Cr10 High Entropy Alloy

G.J. Bi[a*], Z.G. Zhu[a], Y.X. Chew[a], F. L. Ng[a], B. Y. Lee[a]

[a]*Singapore Institute of Manufacturing Technology, 73 Nanyang Drive, Singapore 637662, Singapore*

Abstract

Laser aided additive manufacturing (LAAM) was demonstrated to successfully fabricate bulk Fe50Mn30Co10Cr10 high entropy alloy using pre-alloyed powder. The microstructure and fraction of hexagonal closely-packed (HCP) phase formation due to deformation induced phase transformation (TRIP effect) were characterized using EBSD to analyze phase fraction and twinning. The fabricated samples achieved ultimate tensile strength of 905MPa and 23% elongation under room temperature loading conditions. The as-built $Fe_{50}Mn_{30}Co_{10}Cr_{10}$ samples exhibit both cellular and dendritic microstructure typical of LAAM built parts. The higher mechanical strength and ductility of this HEA material at room temperature is due to dislocation strengthening of the matrix FCC phase, TRIP FCC-HCP phase transformation and twinning formation. The strain hardening behavior, dislocation density with increasing tensile strains will be also discussed in this work.

Keywords: High Entropy alloys; laser metal deposition; additive manufacturing; microstructure; mechanical properties

1. Introduction

Most high entropy alloys or multicomponent alloys, utilize four or more elements in equal or near equal atomic ratio to form single phase alloy stabilized by their large mixing entropies (Yeh, Chen et al. 2004). One of the most commonly studied HEA CoCrFeNiMn, first proposed by (Cantor, Chang et al. 2004) remains thermodynamically stable as a single phase FCC solid solution above 800℃ before small quantities of Cr-rich precipitates forms around annealing temperature of 700℃ at grain boundary, inclusions and pores (Otto, Dlouhý et al. 2016). The predominantly single phase CoCrFeNiMn HEA exhibits good mechanical strength at room temperature, with both enhanced strength and ductility at cryogenic temperatures (Laplanche, Kostka et al. 2016).

With the broadening of the HEA definition driven by on-going studies, there are an expansive range of materials to be studied within the space of multicomponent alloy systems. As mentioned in a review by (Miracle and Senkov 2017), some researchers prefer to classify based on the alloy entropy magnitude (>1.61R), while some call for less restriction in the equimolar definition to consider principal elements with

concentration between 5-35 %, also known as multi-principal elements alloys (MPEA). Another term sometimes used interchangeably with MPEA is the complex concentrated alloys (CCAs), which refers to ternary and quaternary alloys with principal element concentration in excess of 35% (Gorsse, Couzinié et al. 2018). Both MPEA and CCA have less emphasis on developing a single phase solid solution, but focus on characterizing the diverse microstructures and properties instead. In this work, the broad definition of high entropy alloy will be used rather than the initial tighter definition. As such, a four component $Fe_{50}Mn_{30}Co_{10}Cr_{10}$ alloy designed to form two phases (Li, Tasan et al. 2017) for achieving better strength and ductility combination compared to a single phase system will be investigated.

The novel alloy design concept of HEA along with their promising mechanical properties leads to development of alternative fabrication methods using additive manufacturing such as selective laser melting (Zhu, Nguyen et al. 2018) and Laser Aided Additive Manufacturing (LAAM) (Chew, Bi et al. 2019, Tong, Ren et al. 2019). These investigations reported superior yield and ultimate tensile strength but with reduced ductility for HEA fabricated by AM processes compared to arc-melting and casting(Otto, Dlouhý et al. 2013). In addition, it was interesting to note from the earlier cited work on CoCrFeNiMn HEA that, though cooling rates were expected to be significantly higher in SLM compared to LAAM, the yield strength of the different AM samples were rather similar. Slightly higher elongation were observed in the SLM samples relative to those from LAAM process. Hence, further research efforts are necessary in the area of AM processing to enhance the mechanical performances of these new HEA and MPEAs. Understanding the resulting microstructure and mechanical properties are also useful for wider applications of these multi-principal element alloys. Laser Aided Additive Manufacturing is a flexible technology which utilizes blown powder delivery method or wire feeding in some cases to efficiently build bulk materials without having to fill the powder bed. In this work, LAAM will be used to investigate the microstructure and mechanical properties of the transformation induced plasticity (TRIP) $Fe_{50}Mn_{30}Co_{10}Cr_{10}$ high entropy alloy.

2. LAAM Experiment

The bulk $Fe_{50}Mn_{30}Co_{10}Cr_{10}$ alloy was fabricated using the LAAM system developed in SIMTech and the details have been previously reported in (Bi, Chew et al. 2018, Chew, Bi et al. 2019). The argon shielding gas through the coaxial nozzle was delivered to minimize melt-pool oxidation. Argon is also used as carrier gas for the discrete powder jets of pre-alloyed HEA powder with particle size range of $45\mu m - 105\mu m$. The process parameters used in this study are as follows: i) laser beam size of 2.5mm, ii) laser scanning speed of 10mm/s, iii) laser power of 970W, iv) Powder feeding rate of 8.9g/min and v) layer height of 0.5mm. The tensile coupons were wire-cut from a printed block with dimensions 108 mm (length) × 70mm (width) × 6.5mm (height) and the sample dimensions following the guidelines in ASTM standard E8. The tensile property was performed at a strain rate of 10^{-3}/s using a universal Instron-5982 testing system.

The printed samples were cross-sectioned and the final polishing step was performed with Struers 0.05 μm oxide dispersion suspension (OPS). Optical microscope imaging was performed for the as-built samples and SEM with EDS to examined the fractured tensile coupons. EBSD analysis was also performed to map the grain morphology and the phase fractions.

3. Results and Discussion

3.1. Microstructure and EBSD analysis

The optical microscope (OM) image of the as-built LAAM cross-sectioned along the layer height built direction is presented in Fig. 1a and a close-up view of the boxed region is given in Fig. 1b below. The laser

raster scan direction is rotated 90 degrees with each subsequent deposited layer. The step-over or hatch size of 50 % beam diameter is used to deposit material in the transverse direction within a single layer. The described laser pathway will cause partial re-melting of the previous layer and adjacent deposited clad track, giving the complex and mixed microstructure shown in Fig. 1a and Fig. 1b. The microstructure of the layer deposited by laser raster scan direction moving left to right and vice versa with reference to the OM image is discernable by the equiaxed grains. These equiaxed structure are formed at the rearward of the advancing melt-pool and some faint solidification front are marked out using black arrows in Fig 1. For layers deposited by laser scan movement in and out-of-plane, directional solidification with dendritic columnar grains are formed along the elliptical melt-pool boundaries. At the overlap regions, there is a distinctive change in the columnar grain orientation as shown in Fig. 1b. In addition, there are signs of epitaxial grain growth of both equiaxed and dendritic columnar structures which are extended over more than one layer, as shown near the right edge of Fig 1a. This competitive grain growth phenomenon whereby epitaxial grains with orientation more aligned with the thermal gradient direction outgrew those which are less aligned, was also reported in powder bed AM processing of CoCrFeMnNi HEA (Piglione, Dovgyy et al. 2018).

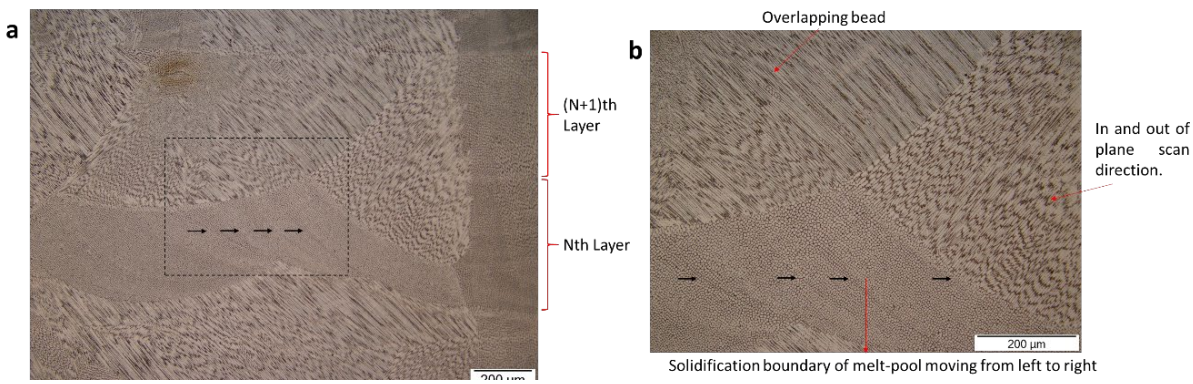

Fig. 1. a) Optical image of the as-built LAAM sample in cross-sectional plane through the building direction. b) Close-up view showing mixture of dendritic columnar and equiaxed grains at the interface between two layers and overlapping passes.

The EBSD analysis results showing the inverse pole figure map is presented in Fig. 2a and Fig. 2b. The EBSD mapping in Fig. 2 consists of a connected neighboring regions from top to bottom along the built direction. The result is consistent with the OM images which showed extended epitaxy grain growth orientation along thermal gradient or built direction near the left edge of the EBSD images. Importantly, the EBSD results revealed that the as-printed LAAM sample does not contain significant amount of initial HCP phase unlike cast samples which were homogenized and water-quenched (Li, Tasan et al. 2017). EDS mapping analysis further indicated that the boundaries of the equiaxed and columnar dendritic structures are deficient in Fe but rich in Mn. No elemental segregation was observed for both Co and Cr in the as-built samples. The elemental segregation may be suppressed by reducing oxidation or increasing cooling rate as segregation of Mn was not observed in SLM processing of similar material.

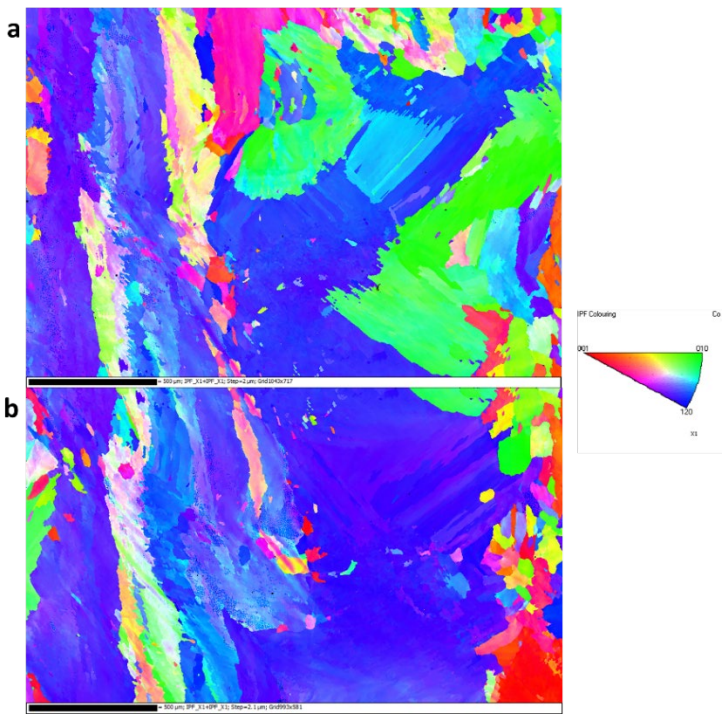

Fig. 2. a) EBSD image showing the inverse pole figure of the as-built sample along the built direction (top) and b) bottom.

3.2. Mechanical Properties

The tensile test result of the LAAM built $Fe_{50}Mn_{30}Co_{10}Cr_{10}$ samples under room temperature is plotted in Fig. 3a. A total of 3 samples has been tested and the observed average yield strength (σ_y), ultimate tensile strength (σ_{UTS}) and elongation ε_{UTS} are approximately σ_y=652MPa, σ_{UTS}=905MPa and ε_{UTS}=22.7%. Both the strength and ductility are higher than the previously reported equimolar single phase CoCrFeNiMn fabricated using LAAM process (Chew, Bi et al. 2019). This is also significantly different from the mechanical properties of cast samples whereby the reported yield and tensile strength are 250MPa and 720MPa with initial HCP phase fraction of 28% (grain size $\sim 45\mu m$) and elongation of approximately 50% (Li, Tasan et al. 2017). There exists a ductility and strength trade-off which is commonly observed in additive manufactured samples. This may be partly due to the dislocations present in the LAAM sample, even prior to loading which reduces dislocation mobility. The SEM image of the fractured surface is given in Fig. 3b. The fractured surface shows numerous ductile dimples with embedded sub-micron particles. These particles act as void nucleation sites and are likely detrimental to ductility.

The EDX analysis shows that the particle contains high weight percentage of Mn of about 48% with small amount of impurities such as Silicon and Aluminum. The Mn-rich particles may be caused by oxidation and such observation was also reported by other authors (Tong, Ren et al. 2019), as this is difficult to avoid with the lack controlled environment when processing material with high Mn content. It is also noted that the observed fractured surface characteristic is very similar to that of the CoCrFeNiMn HEA.

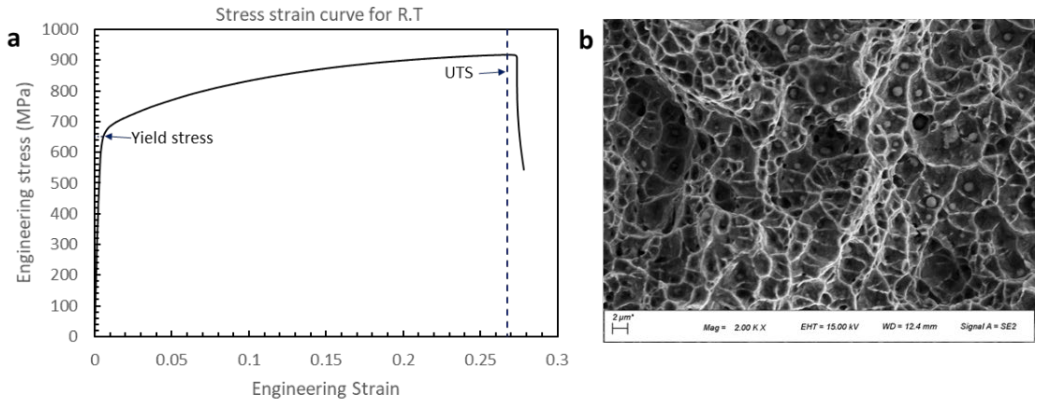

Fig. 3. a) Engineering stress strain curve for as-built LAAM sample under room temperature b) SEM image of fractured surface.

The ESBD results of the fractured sample along the y-z plane where y direction is the tensile loading direction and z refers to the built direction is given in Fig. 4 below. The ESBD results confirms both the formation of HCP phase and twinning within the FCC phase. Fig 4a shows the inverse pole figure for both the FCC phase and HCP phase while Fig. 4b illustrates the phase fraction between the two phases indicated by blue region for FCC and red region for HCP phases. The twin boundaries are indicated by blue lines and large angle grain boundaries $> 15°$ are indicated by black lines in Fig. 4b. The HCP phase are formed with the FCC matrix phase and are sparsely distributed as needle-like structures. It was previously reported that this material undergoes FCC-HCP transformation readily with the TRIP effect and can reach as high as 75% HCP phase before fracture for cast samples (Fu, Bei et al. 2018). However, the average HCP phase fraction in LAAM fractured sample is only approximately 7%. This can perhaps explain the low elongation in the LAAM sample as the activation of twinning, dislocation and stacking faults in the HCP are mechanisms for further plastic deformation (Fu, Bei et al. 2018). This low HCP phase fraction in the fractured sample also implies the strengthening mechanism in this LAAM sample is different from the reported TRIP-assisted FCC matrix to HCP transformation.

The $Fe_{50}Mn_{30}Co_{10}Cr_{10}$ HEA excellent combination of strength and ductility is also known to be insensitive to strain rates and different grain sizes between 2.8 and $38\mu m$ (Basu, Li et al. 2018). It was also reported that having higher initial HCP phase fraction can increase both strength and ductility. In the LAAM sample, the initial HCP phase fraction appears to be less than 1%. Thus, the main strengthening mechanism in this work is attributed to the increasing dislocation density, formation of twins within the FCC phase and partially due to the TRIP effect. The low initial HCP phase fraction prior to tensile loading is similar to that observed in carbon-doped interstitial high-entropy alloy (iHEA) with composition of $Fe_{49.5}Mn_{30}Co_{10}Cr_{10}C_{0.5}$ with joint TWIP (Twinning-Induced Plasticity) and TRIP effects (Li, Tasan et al. 2017). Nonetheless, even under room temperature loading of cast iHEA, the HCP phase fraction is approximately 30% for fine grains sample (Wang, Lu et al. 2019). The lack of FCC matrix to HCP transformation may be due suppressed by other trace elements which maybe be present in the pre-alloyed powder used in this work. Further studies will focus on the effects of larger grain size observed in LAAM samples due to the epitaxial grain growth and their effects on strengthening behavior.

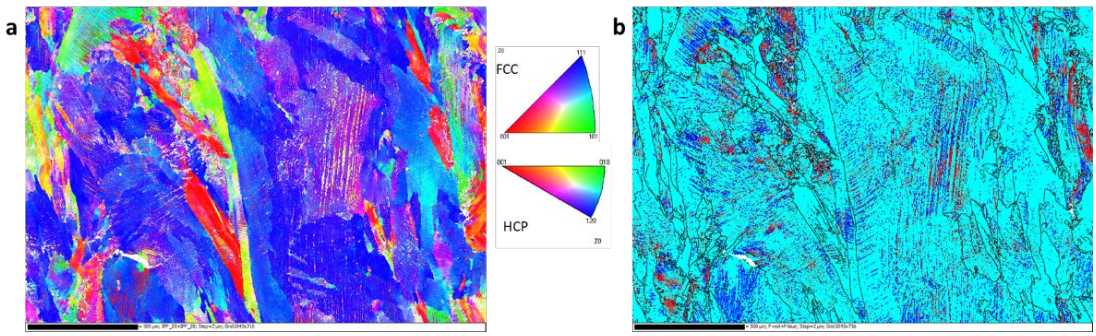

Fig. 4. a) Inverse pole figure map of the FCC and HCP phase, b) Phase fraction map showing large angle phase boundary and twinning.

4. Conclusion

The mechanical properties and microstructure of bulk $Fe_{50}Mn_{30}Co_{10}Cr_{10}$ fabricated using the LAAM process with blown powder delivery had been studied. Cross-section OM images showed low porosity level with no observable micro-cracks in the LAAM sample. The key characteristics in the as-built LAAM microstructure is the mixed equiaxed and columnar dendritic grains formed by alternating laser scan direction and overlapping passes combined with epitaxial grain growth extending over several layers. Twinning within the FCC phase had been observed in the EBSD results of the fractured test coupon even under room temperature. Approximately 7% HCP phase was formed within prior FCC grains due to TRIP. The main finding is that the yield and ultimate tensile strength of this material is significantly higher than single FCC HEA (CoCrFeNiMn), dual-phase HEA $Fe_{50}Mn_{30}Co_{10}Cr_{10}$ and even for iHEA $Fe_{49.5}Mn_{30}Co_{10}Cr_{10}C_{0.5}$ which were manufactured by casting. One notable difference is also the significantly lower elongation (23%) in the LAAM sample. Future studies will investigate the effect of grain growth orientation in LAAM built part on the strengthening mechanism.

Acknowledgement

This research was supported by Agency for Science, Technology and Research (A*Star), Republic of Singapore, under the IAF-PP program “Integrated large format hybrid manufacturing using wire-fed and powder-blown technology for LAAM process”, Grant No: A1893a0031.

References

Yeh, J.-W., S.-K. Chen, S.-J. Lin, J.-Y. Gan, T.-S. Chin, T.-T. Shun, C.-H. Tsau and S.-Y. Chang (2004). "Nanostructured High-Entropy Alloys with Multiple Principal Elements: Novel Alloy Design Concepts and Outcomes." Advanced Engineering Materials 6(5): 299-303.

Cantor, B., I. T. H. Chang, P. Knight and A. J. B. Vincent (2004). "Microstructural development in equiatomic multicomponent alloys." Materials Science and Engineering: A 375-377: 213-218.

Otto, F., A. Dlouhý, K. G. Pradeep, M. Kuběnová, D. Raabe, G. Eggeler and E. P. George (2016). "Decomposition of the single-phase high-entropy alloy CrMnFeCoNi after prolonged anneals at intermediate temperatures." Acta Materialia 112: 40-52.

Laplanche, G., A. Kostka, O. M. Horst, G. Eggeler and E. P. George (2016). "Microstructure evolution and critical stress for twinning in the CrMnFeCoNi high-entropy alloy." Acta Materialia 118: 152-163.

Miracle, D. B. and O. N. Senkov (2017). "A critical review of high entropy alloys and related concepts." Acta Materialia 122: 448-511.

Gorsse, S., J.-P. Couzinié and D. B. Miracle (2018). "From high-entropy alloys to complex concentrated alloys." Comptes Rendus Physique 19(8): 721-736.

Li, Z., C. C. Tasan, K. G. Pradeep and D. Raabe (2017). "A TRIP-assisted dual-phase high-entropy alloy: Grain size and phase fraction effects on deformation behavior." Acta Materialia 131: 323-335.

Zhu, Z. G., Q. B. Nguyen, F. L. Ng, X. H. An, X. Z. Liao, P. K. Liaw, S. M. L. Nai and J. Wei (2018). "Hierarchical microstructure and strengthening mechanisms of a CoCrFeNiMn high entropy alloy additively manufactured by selective laser melting." Scripta Materialia 154: 20-24.

Chew, Y., G. J. Bi, Z. G. Zhu, F. L. Ng, F. Weng, S. B. Liu, S. M. L. Nai and B. Y. Lee (2019). "Microstructure and enhanced strength of laser aided additive manufactured CoCrFeNiMn high entropy alloy." Materials Science and Engineering: A 744: 137-144.

Tong, Z., X. Ren, J. Jiao, W. Zhou, Y. Ren, Y. Ye, E. A. Larson and J. Gu (2019). "Laser additive manufacturing of FeCrCoMnNi high-entropy alloy: Effect of heat treatment on microstructure, residual stress and mechanical property." Journal of Alloys and Compounds 785: 1144-1159.

Otto, F., A. Dlouhý, C. Somsen, H. Bei, G. Eggeler and E. P. George (2013). "The influences of temperature and microstructure on the tensile properties of a CoCrFeMnNi high-entropy alloy." Acta Materialia 61(15): 5743-5755.

Bi, G., Y. Chew, F. Weng, Z. Zhu, F. L. Ng and B. Y. Lee (2018). Process study and characterization of properties of FerCrNiMnCo high-entropy alloys fabricated by laser-aided additive manufacturing, SPIE.

Piglione, A., B. Dovgyy, C. Liu, C. M. Gourlay, P. A. Hooper and M. S. Pham (2018). "Printability and microstructure of the CoCrFeMnNi high-entropy alloy fabricated by laser powder bed fusion." Materials Letters 224: 22-25.

Fu, S., H. Bei, Y. Chen, T. K. Liu, D. Yu and K. An (2018). "Deformation mechanisms and work-hardening behavior of transformation-induced plasticity high entropy alloys by in -situ neutron diffraction." Materials Research Letters 6(11): 620-626.

Basu, S., Z. Li, K. G. Pradeep and D. Raabe (2018). "Strain rate sensitivity of a TRIP-assisted dual-phase high-entropy alloy." Frontiers in Materials Structural Materials 5(30): 1-10.

Li, Z., C. C. Tasan, H. Springer, B. Gault and D. Raabe (2017). "Interstitial atoms enable joint twinning and transformation induced plasticity in strong and ductile high-entropy alloys." Scientific Reports 7: 40704.

Wang, Z., W. Lu, D. Raabe and Z. Li (2019). "On the mechanism of extraordinary strain hardening in an interstitial high-entropy alloy under cryogenic conditions." Journal of Alloys and Compounds 781: 734-743.